ISSN 0208-7774 TRIBOLOGIA 1/2023 p. 27–40
DOI: 10.5604/01.3001.0016.2931

Michał BEMBENEK[*], Janusz KRAWCZYK[**], Krzysztof ZAGÓRSKI[***], Jan PAWLIK[****]

ON THE WEAR MECHANISM OF HIGH-CHROMIUM GYRATORY CRUSHER MANTLE LINING IN TERMS OF THE ASSESSMENT OF THE USED MATERIAL

ANALIZA ZUŻYCIA STOŻKA WEWNĘTRZNEGO KRUSZARKI STOŻKOWEJ POD KĄTEM OCENY ZASTOSOWANEGO MATERIAŁU

Key words: gyratory crusher, erosion wear mechanism, high-chromium cast steel.

Abstract: After the rock is excavated in bulky chunks, it must be processed into fractions usable by diverse branches of industry. There are many approaches to achieving a fine aggregate, and the gyratory crusher is often preferable. Alas, since its working surfaces are subjected to heavy loads of abrasive material, the lining of the gyratory crusher is prone to specific geometry degeneration mechanisms. The authors subjected the mantle lining to a series of tests, such as metallurgical microstructure analysis, chemical composition and hardness evaluation and X-ray examination. Although most mantles are manufactured from the high-manganese Hadfield steel family, the lining was fabricated from high-chromium hypoeutectic white cast steel with a white iron structure. The difference in the chosen material's chemical composition resulted in an uncommon wear mechanism with visible inclined craters emerging in the lower part of the cone, where erosive, dynamically-moving particles were concentrated.

Słowa kluczowe: kruszarka stożkowa, mechanizm zużycia erozyjnego, staliwo wysokochromowe.

Streszczenie: Po wydobyciu skały w dużych kawałkach wymaga ona przetworzenia na frakcje nadające się do wykorzystania przez różne gałęzie przemysłu. Istnieje wiele sposobów na uzyskanie drobnego kruszywa, a kruszarka stożkowa jest często preferowaną opcją. Niestety, jej powierzchnie robocze poddawane są dużym obciążeniom ściernym, co skutkuje tym, że wykładzina kruszarki stożkowej jest podatna na specyficzne mechanizmy degeneracji geometrii. Autorzy poddali wyłożenie stożka szeregowi badań, m.in. analizie mikrostruktury, ocenie składu chemicznego, rentgenowskiej analizie fazowej i twardości w odniesieniu do właściwości tribologicznych na podstawie analizy mechanizmu zużycia. Większość stożków jest wykonywana ze stali wysokomanganowej rodziny Hadfielda, w tym przypadku wyłożenie zostało wykonane z wysokochromowej, podeutektycznego staliwa o strukturze odpowiadającej żeliwu białemu. Zastosowany materiał spowodował występowanie charakterystycznego mechanizmu zużycia w postaci tworzenia się kraterów, gdzie zużycie erozyjne koncentruje się w dolnej części stożka, przy której koncentruje się oddziaływanie większych dynamicznie przemieszczających się cząstek.

INTRODUCTION

Almost all of the vital for human development elements of the periodic table can be found in the Earth's crust; however, it requires much effort before they become usable. The raw minerals in the form of rocks have to be extracted with the help of the mining industry and processed into appropriate geometric forms to eventually become a product of value – from toothpaste to mixed concrete **[L. 1]**.

[*] ORCID: 0000-0002-7665-8058. Faculty of Mechanical Engineering and Robotics, AGH University of Science and Technology, A. Mickiewicza 30 Ave., 30-059 Kraków, Poland; e-mail: bembenek@agh.edu.pl.
[**] ORCID: 0000-0002-7893-1177. Faculty of Metals Engineering and Industrial Computer Science, AGH University of Science and Technology, A. Mickiewicza 30 Ave., 30-059 Kraków, Poland; e-mail: jkrawcz@agh.edu.pl.
[***] ORCID: 0000-0002-1898-8307. Faculty of Mechanical Engineering and Robotics, AGH University of Science and Technology, A. Mickiewicza 30 Ave., 30-059 Kraków, Poland; e-mail: zagkrzys@agh.edu.pl.
[****] ORCID: 0000-0002-1914-9900. Faculty of Mechanical Engineering and Robotics, AGH University of Science and Technology, A. Mickiewicza 30 Ave., 30-059 Kraków, Poland; e-mail: jan.pawlik@agh.edu.pl.

The large chunks of extracted rock material are transported to the processing station, which in a schematic simplification is a set of particular crushing, conveying and screening units. The crushing facility usually consists of a set of different crushers. The crushing procedure is divided into subsequent steps in most conventional mineral processing companies. Jaw crushers are popular for the primary crushing step **[L. 2–4]**. In the same manner, the secondary and tertiary step of the mineral particle size reduction process relies on gyratory crushers **[L. 5–7]**. The finer grain requires an additional fourth step, fulfilled either with smaller-gapped cone crushers, vertical shaft impactors (VSI), or even roll-presses or beater mills **[L. 8, 9]**. All of the stages struggle with specific wear and maintenance issues, and this paper focuses on the wear of a gyratory crusher mantle lining.

The principle of operation of a gyratory crusher relies on the eccentrically driven cone, placed inside a fixed conical casing, named "concave". The crushers are designed in a manner that allows the mantle shaft to swing slightly during the eccentric rotation. **[L. 10]**. While the mantle is moving, the gap between the mantle and concave surface varies from a state called "OSS" to CSS" – Open Side Setting and Closed Side Setting, respectively. The OSS is the distance which is directly linked to the maximal size of crushed particles. The principle of operation and normal wear pattern is visually explained in **Figure 1**.

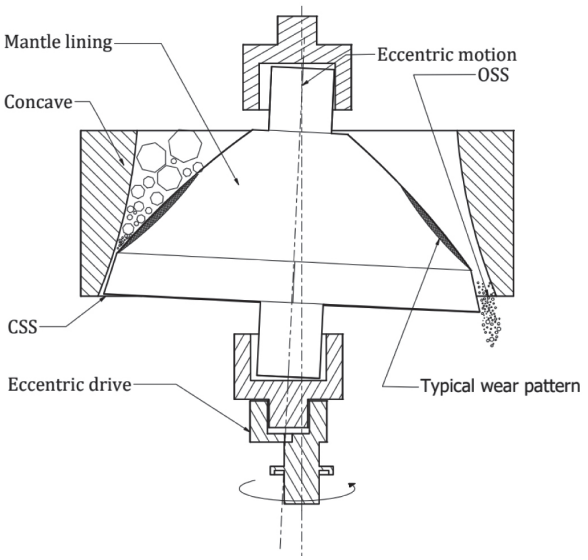

Fig. 1. Schematic principle of operation of a gyratory crusher with an eccentric motion

Rys. 1. Schematyczna zasada działania kruszarki stożkowej z ruchem mimośrodowym

As both the concave and mantle are subjected to strong loads of abrasive mineral feed, the proper selection of material is crucial for the gyratory crusher's reliability. The most common material used for those parts is cast steel from the manganese-rich Hadfield steel family, which expresses its work-hardening behaviour **[L. 11–13]**. Considering the operating conditions, the self-reinforcement property of the micro-twinning of the crystals in the microstructure seems to be the most suitable approach for the rock pulverising process **[L. 14]**. Regarding the evaluation of the mantle's lining performance model has been proposed by many different research teams **[L. 15]**. For instance, Cleary et al. **[L. 16]** have developed a method of geometrical evaluation, which may be a supplementary approach to the more widely used Discrete Element Method (DEM). Ma et al. **[L. 17]**, based on previous findings of Lindqvist and Evertsson **[L. 18, 19]**, performed extensive laboratory and on-site tests, which helped to develop a pressure model based on Particle Size Distribution (PSD). Despite being an interesting approach, their findings did not consider the wear mechanism of a particular material, as the sole material parameter was the hardness. However, Hadfield steel is merely one example of heavy-duty steel. In this paper, the Authors study the gyratory crusher mantle, fabricated with high-chromium steel, which is another example of wear-, erosion- and corrosion-resistant material **[L. 20–22]**. The studied part, primarily used in industrial conditions, presents divergent damage behaviour. The authors utilise several physical metallurgy methods in an attempt to explain the unusual wear mechanism of the aforementioned part. Additionally, Hadfield steels are considered as being difficult to regenerate via hardfacing since they require several layers, including a buffer layer **[L. 23]**. In the case of the high-chromium cast steels, they are considered easier to handle while building up such wear-resistant layers **[L. 24]**. That kind of regeneration technique can greatly enhance the lifespan of a part subjected to erosion **[L. 25, 26]**. Moreover, Hadfield's cast steel is not resistant to erosive wear due to the influence of small, low-energy fractions that do not strengthen by micro-twinning deformation **[L. 27]**. High-chromium iron alloys should be characterised by greater wear resistance in the above-mentioned conditions **[L. 27]**. Hence, this type of material

should be effective in interacting with various fractions of crushed material in this device.

In this paper, the Authors attempt to identify the exact composition of the material used for gyratory crusher mantle lining fabrication and inspect its properties in order to identify the wear mechanism and possible defects. Extensive microstructure analysis of different part areas, Rockwell hardness testing and X-Ray phase analysis, are the main constituents of the scope of the current study.

MATERIALS AND METHODS

The sample studied in this paper is a worn mantle lining from the gyratory crusher. This was prepared by first cutting out a bigger chunk of the remaining mantle body and afterwards cutting out a region unaffected by the cutting heat. The original geometry was replicated by 3D scanning (**Fig. 2a**), which allowed for further manufacturing process documentation preparation (**Fig. 2b**).

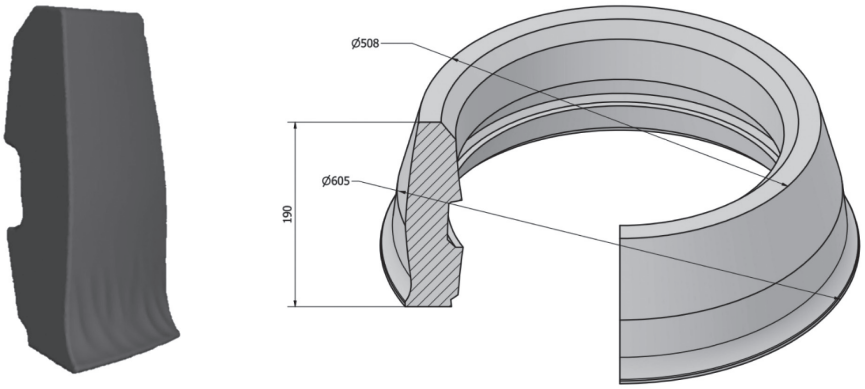

(a) (b)

Fig. 2. Drawing of the original gyratory crusher mantle (a) depicts the 3D-scan, (b) the re-created mantle model
Rys. 2. Rysunek oryginalnego płaszcza kruszarki stożkowej (a) skan 3D, (b) odtworzony model płaszcza

The smaller chunk was diced on a water-abrasive cutter into further pieces, prepared for a series of tests. **Figure 3** depicts the initial cut-out with rectangular zones described with a black marker, indicating the particular test destination. The inspection contained the following steps:

1. Macroscopic visual evaluation and wear description.
2. Chemical composition, identified with the Foundry-Master (WAS) optical emission spectrometer (Hitachi, Tokyo, Japan). The measurements were repeated three times.
3. Metallographic analysis of the polished and etched specimen with Carl Zeiss Axiovert 200 MAT microscope (Carl Zeiss Microscopy Deutschland GmbH, Oberkochen, Germany). The used etchant composition was 2% HF + 4%HNO_3 + 94% H_2O. Volumetric carbide share was estimated via the point method with 10x10 mesh, adjusted to the order of optical magnification.
4. X-Ray phase analysis, conducted with D8 Advance diffractometer (Bruker, Massachusetts, USA).
5. Metallographic analysis of working surface specimen with Carl Zeiss Axiovert 200 MAT microscope (Carl Zeiss Microscopy Deutschland GmbH, Oberkochen, Germany).
6. Rockwell hardness test – 18 measurements with a 1 mm span, performed on two lines perpendicular to the non-working surface. Hardness measurements were made using the Zwick/Roell ZHU 187.5 hardness tester (ZwickRoell GmbH & Co. KG, Ulm, Germany).
7. Superficial SEM analysis. The tests were conducted using a scanning electron microscope (Japan Electron Optics Laboratory Co., Ltd., Tokyo, Japan).

Table 1. Sample enumeration
Tabela 1. Oznaczenie próbek

Sample indicator	Conducted test
A1, A3, A5-A7	Metallographic inspection
A4, B1	Chemical analysis
B1-B7	Surface SEM analysis

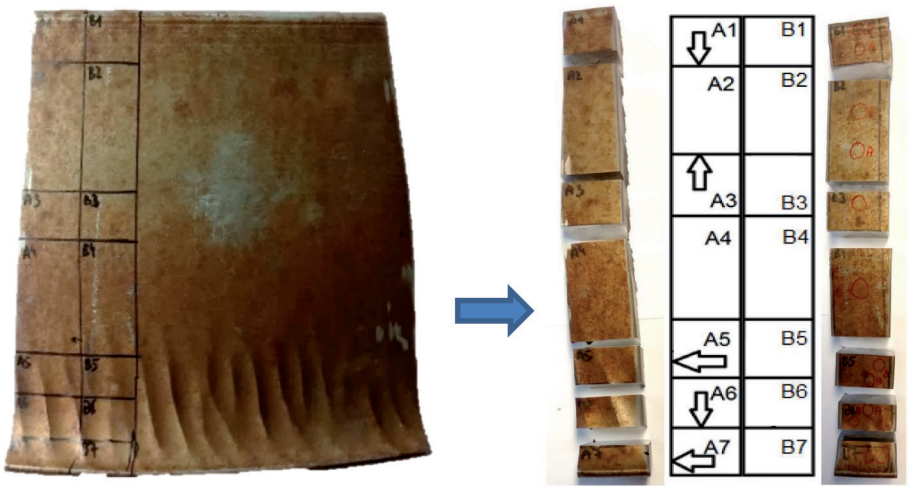

Fig. 3. Picture of the inspected gyratory crusher mantle cut-out. The black grid represents markers for further sample preparation

Rys. 3. Zdjęcie pobrania próbek ze stożka kruszarki stożkowej. Czarna siatka przedstawia oznaczenia do dalszego przygotowania próbki

A preliminary chemical analysis of the working surface (sample B1) was carried out with the use of energy dispersive X-Ray analysis (EDS). It revealed that the gyratory crusher was likely to operate in an environment rich in silicon oxide; thus, the authors could confirm that the machine dealt with granite crushing.

Table 2. Chemical composition of the surface layer

Tabela 2. Skład chemiczny warstwy wierzchniej

Chemical element	Mass %	Stechiometric %
O	48	–
Si	27	52
Fe	5	29
Cr	6	12
Al	4	7

RESULTS

Macroscopic visual inspection and wear description

The mantle lining presents a volumetric loss in the expected area at the bottom of the lining cone. On the working surface area subjected to the highest loads, one can notice the vertical wear marks. The motion, fulfilled by the mantle is gyratory; thus, the grooves are slightly inclined towards the main axis of the mantle shaft (**Fig. 4**). The measured angle of inclination varies between 10.95° and 13.12°

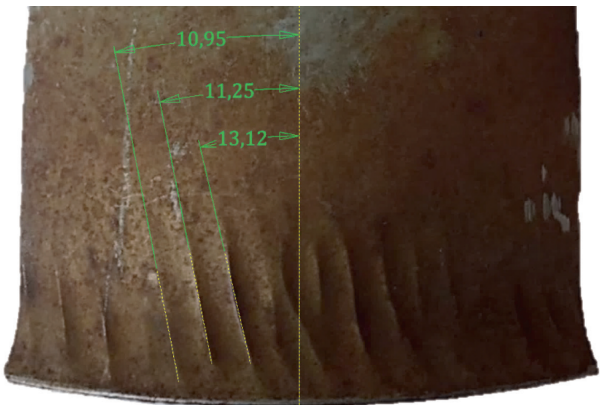

Fig. 4. Close-up macroscopic picture of the vertically inclined grooves resulting from wear

Rys. 4. Widok makroskopowy rowków nachylonych w pionie, powstałych w wyniku zużycia

Chemical composition analysis

The material used for mantle fabrication was declared EN-GJN–HV600 (XCr23) steel, which was later confirmed during the chemical composition analysis. The analysis was firstly carried out via energy-dispersive X-ray spectroscopy, yet since this method does not detect light elements – such

as carbon – additional chemical spark analysis was also performed. The results are presented in **Table 3** (EDS) and **Table 4** (full analysis). According to the standard EN 12513:2011, this material belongs to the high-chromium abrasion-resistant cast iron.

Table 3. EDS-based analysis of chemical composition
Tabela 3. Analiza EDS składu chemicznego

Chemical element	%	Mass %
Fe	56	58
Cr	42	40
Mo	1	2
Si	1	1

Table 4. Complete chemical analysis
Tabela 4. Pełna analiza chemiczna

Chemical element	Mass %	Mass % according to EN 12513:2011
C	2.44 ±0.04	1.80–3.60
Cr	24.40 ±0.24	23.00–28.00
Mo	0.83 ±0.01	max 3.00
Mn	0.75 ±0.01	0.50–1.50
Si	0.48 ±0.01	max 1.0
Ni	0.29 ±0.01	max 2.0
P	0.04±0.01	max 0.08
S	0.04±0.01	max 0.08
Cu	0.03±0.01	max 1.2

Metallographic analysis of the polished and etched cut-outs

The inspected specimen appeared to have the structure of hypoeutectic white cast iron. The microscopic images of each identified phase below refer to each examined sample.

The material consists of areas of differently oriented sets of dendrites, where those sets will be further referred to as crystallites. **Figure 5a** (sample A5) shows the crystallite boundaries. The area of particular crystallite corresponds with the austenite, solidifying from the liquidus phase, as seen in **Figure 5c**. The eutectic phase, made out primarily of austenite and primary carbides, was identified in the inter-dendritic space. In the process of further cooling, secondary carbides emerged, and the result can be seen in **Figure 5e**. Further heat treatment resulted in a martensite structure present, which is visible. During austenite cooling, some of the secondary carbides have been attached to the primary carbides, especially in the areas of former eutectic. Due to more intensive etching, the authors could observe the effects of martensite tempering in sample A7 (**Fig. 5b, d, f**). It is presented in the, especially in subfigures (f). Specific etching of sample A1 enabled the authors to observe acicular (**Fig. 5 g**). The average length of the occurring dendrites was calculated to be approximately 623 μm. Also, in **Figure 5h**, lamellar and acicular eutectic morphology can be distinguished. Some lamellae are arranged radially, while others are organised parallelly.

When sample A5 was inspected, a few cracks were captured, which are visible in **Figures 6 a** and **b**. After stitching the singular microscopic images and drawing perimeters of the crystallites (**Fig. 6a** – blue, dashed line), the cracks' geometry appeared to run along the crystallite boundaries. It is a highly undesirable occurrence since whether the crack is initiated on the surface of the mantle lining, it can easily propagate deep into the part.

Another possible reason behind decreasing the wear resistance of the studied part may be the occurring porosity. The pores are visible in **Fig. 7**. They probably emerged during the rapid cooling of the freshly-cast part, when the crystallising material reduced its volume, causing internal shrinkage, cracks and discontinuities. Another possible reason for the existence of the pores is the quenching stress, where the temperature difference along the part cross-section was too high (or the cooling process was carried out too fast). In order to prevent inter-dendritic porosity near the surface, longer cooling periods could be introduced. Supposing the pores occur in the internal parts of the lining, they should not affect the operational parameters of the part negatively since by the time the wear-sensitive volume is reached, the geometry of the cone will require replacing, nevertheless.

Based on the observations, the Authors claim that the volumetric share of the primary carbides is approx. 36% (±5%), and the share of the secondary carbides is at approx. 28% ±5%.

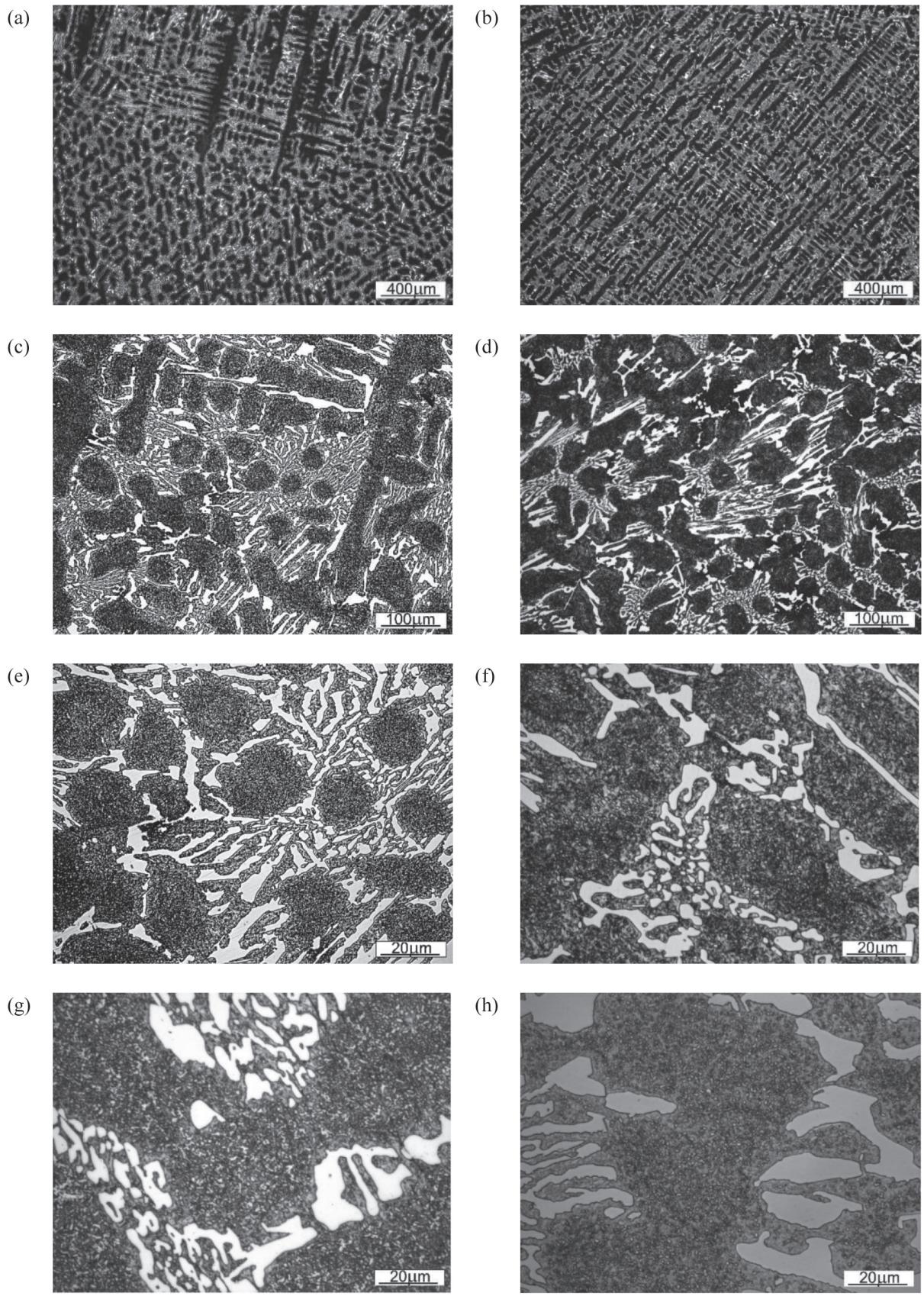

Fig. 5. Microstructure of the sample: A5 (a), (c) and (e) with different magnifications, A7 (b), (d), and (f) with different magnifications, A1 (g) and A3 (h)

Rys. 5. Mikrostruktura próbki: A5 (a), (c) i (e) przy różnym powiększeniu, A7 (b), (d) i (f) przy różnym powiększeniu, A1 (g) i A3 (h)

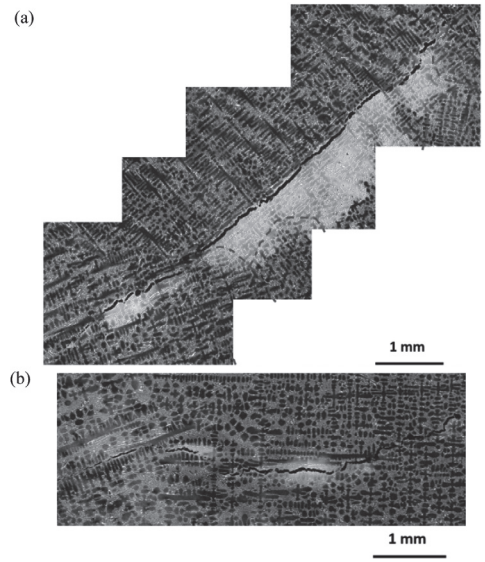

Fig. 6. Cracks were observed during the inspection of sample A5: (a) shows crack propagation along the crystalline boundaries, and (b) shows the change of the crack's path due to differently oriented dendrites

Rys. 6. Pęknięcia zaobserwowane podczas badania próbki A5: (a) pokazuje propagację pęknięcia wzdłuż granic krystalicznych, (b) pokazuje zmianę toru pęknięcia spowodowaną różnie zorientowanymi dendrytami

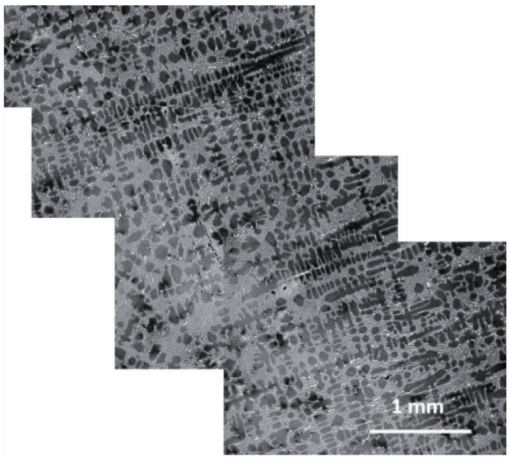

Fig. 7. The porosity of sample A5 is due to casting shrinkage or quenching stresses

Rys. 7. Porowatość próbki A5 spowodowana skurczem odlewniczym lub naprężeniami hartowniczymi

X-Ray phase analysis

The phase composition of the studied part was evaluated with the aid of Bruker D8 Advance diffractometer. The diffractograms were compared with the ideal element response, depicted as dashed lines in the subfigures (a)-(g) of **Figure 8**.

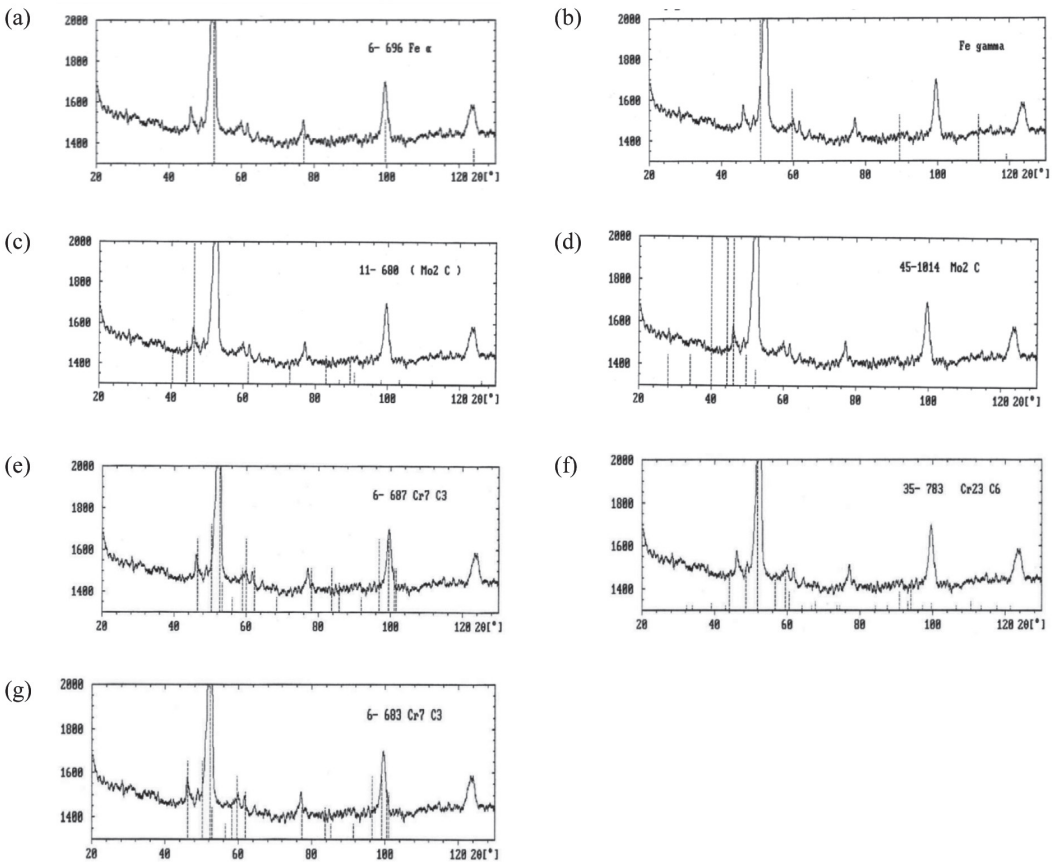

Fig. 8. Diffractograms of the studied material with vertical dashed lines, marking the match with certain phases

Rys. 8. Dyfraktogramy badanego materiału liniami pionowymi przerywanymi, zaznaczającymi dopasowanie określonymi fazami

Subfigure (a) contains the peaks of α-iron, which may refer to the cubic martensite present in the alloy. In subfigure (b), one can see the presence of γ-iron, which means that austenite also constitutes 2% of the total phase composition. Noteworthy, this phase is the retained austenite, indicating that the part was subjected to heat treatment. The remaining subfigures (c) and (d) show matching peaks for the Mo_2C carbides, while (e) and (f) correspond to the chromium carbides Cr_7C_3. The matching differences can be explained by the fact that the carbide existing in the current alloy is described as $(Fe, Cr)_7C_3$. This is the main carbide constituent of the mantle lining. The last subfigure (g) shows the low amount of $Cr_{23}C_6$ carbides, which also exist in the alloy in the $(Fe, Cr)_{23}C_6$ stochiometric composition.

Analysis of the working surface

The microstructure inspection of the superficial layer was divided into two parts: one inspection of the working surface and the second observation of the non-exploited area. That enabled the Authors to compare and assess the impact of wear on the studied part.

Considering the non-working surface, no areas of columnar phase were observed. Some noticed contamination and unevenness are probably a result of issues with the roughness of the casting mould. **Figure 9** depicts the described microstructural properties.

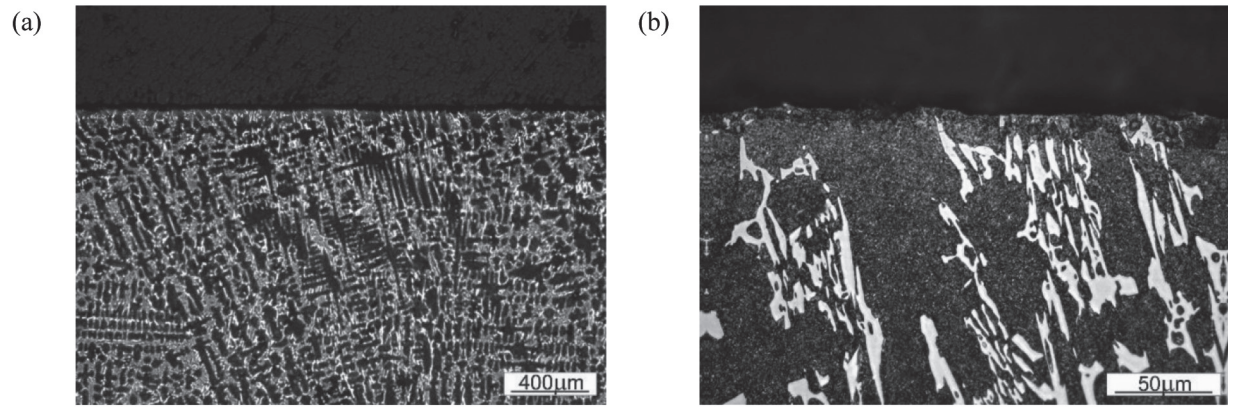

Fig. 9. Microstructure of the superficial layer of the not-exploited surface of the mantle lining (a) the general view, (b) depicts the surface roughness, being a consequence of ceramic casting form

Rys. 9. Mikrostruktura warstwy powierzchniowej nieeksploatowanej powierzchni okładziny płaszcza (a) widok ogólny, (b) chropowatość powierzchni będącą konsekwencją formy odlewu ceramicznego

During the observations of the exploited surface, a binary role of the primary carbides was noticed. On the one hand, it is visible that the primary carbides diminish the abrasive wear (**Fig. 10a**, area 1), yet on the other hand, the observed cracks are propagating along the carbide lattice (**Fig. 10a**, area 2). A similar crack propagation mechanism is also visible in **Figures 10c** and d (which presents the same area but with different magnification). The outcome of superficial mechanical impact also depends on the dendrites' arrangement, where **Figure 10b** is one of the best examples found. The porosity, seen in **Figures 10e** and **f**, is another possible factor that sets the upper limit for wear resistance.

The microstructural examination of the polished and etched mantle samples provided some information about the material and its wear behaviour causes; nonetheless, the authors also wanted to perform an areological analysis. The captured images in **Figure 11** confirm the previously found worn material defects. In subfigures (a)-(f), one can observe the divergent reaction to abrasion of the particular material phases, subfigures (a), (b) and (d) show the occurrence of cracks and subfigure (e) depict craters.

Some micro-cracks were observed on the material surface, as seen in **Figure 12**. The cracks tend to propagate along the crystallite boundaries.

During the operation of the machine, the mantle lining was periodically eroded. The cavities collected the products of erosion, and some build-ups started to occur. The process continued with build-up ripping, resulting in visible craters. Some exemplary craters are presented in **Figure 13**, marked with red circles.

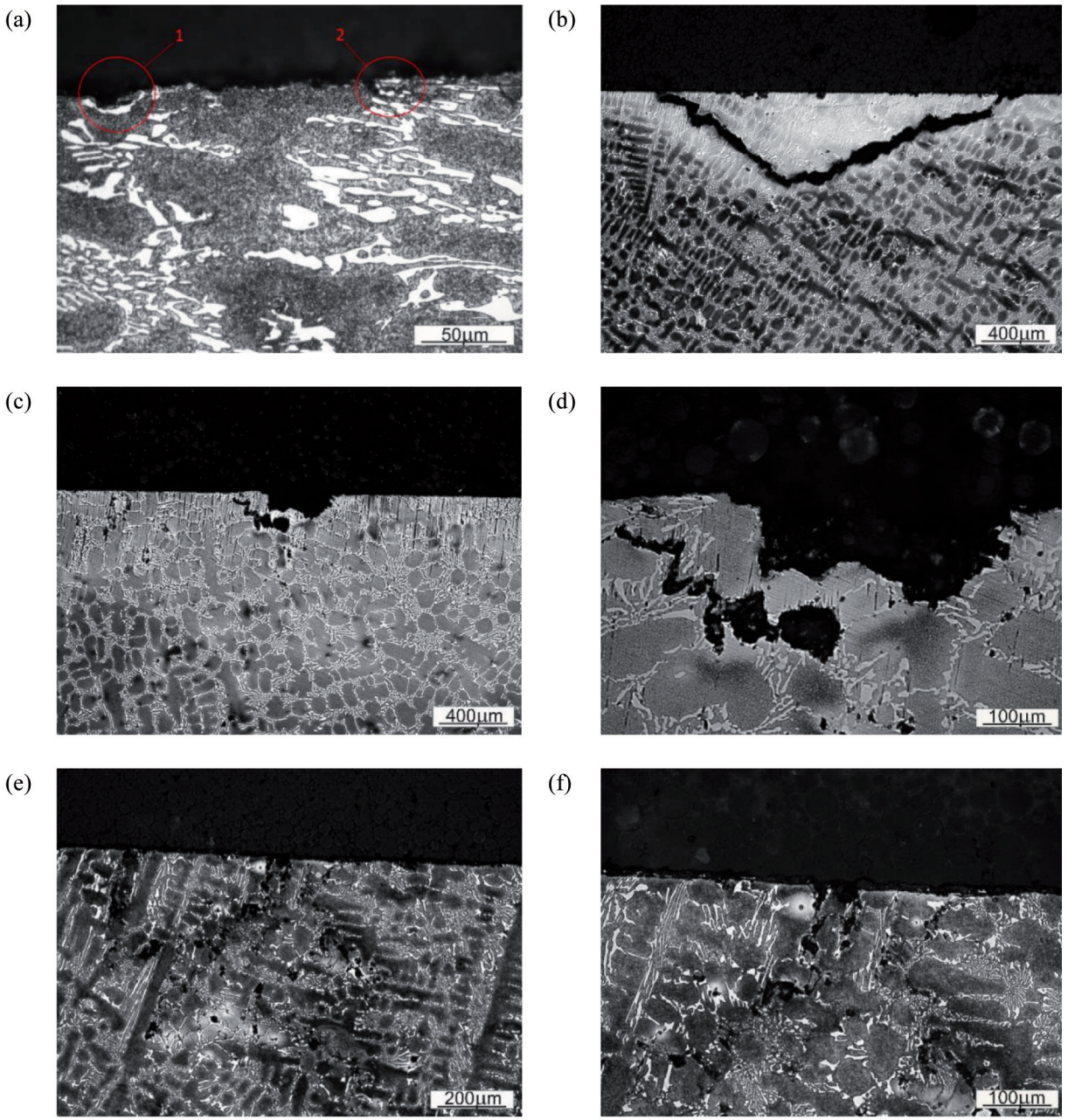

Fig. 10. Microstructure of the exploited surface of the studied part: (a)-(c) cracks propagating along the carbide lattice, (d) crack propagating along the dendrites, (e), (f) depicts porosity

Rys. 10. Mikrostruktura eksploatowanej powierzchni badanej części: (a)-(c) pęknięcia propagujące się wzdłuż siatki węglikowej, (d) pęknięcia propagujące wzdłuż dendrytów, (e), (f) porowatość

The images collected in **Figure 14** were captured at an angle to the surface in order to highlight the ploughs and scratches occurring on the B7-A and B7-B samples. Those samples belong to the mantle lining region exposed to fine-grained, crushed abrasive material. In the areas with smaller hardness values, the abrasive wear occurs more rapidly, which afterwards leads to deep creases. The crease partially acts as a funnel, which concentrates the crushed material, further leading to more intensive wear in the particular creased region.

In order to confirm the assumed wear mechanism, the Authors compared microscopic and SEM images of the carefully located same regions of samples. Inspecting the analogue regions of sample B1-A (**Fig. 15**), one can notice that the most

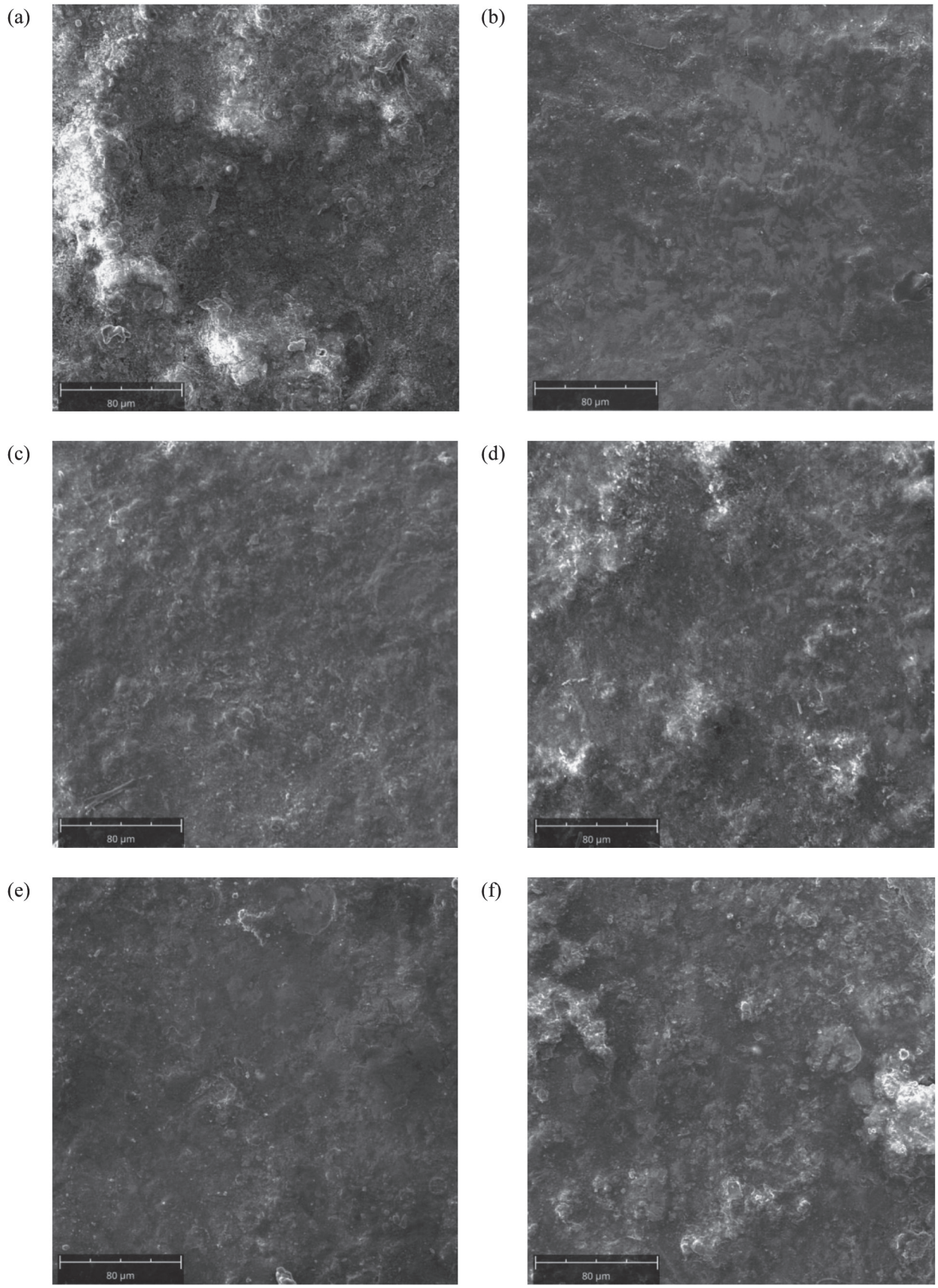

Fig. 11. Areological analysis of the material surface: (a) Sample B1-B, (b) B2-B, (c) B2-B, (d) B3, (e) B6-A and (f) B6-B
Rys. 11. Analiza areologiczna powierzchni materiału (a) próbki B1-B, (b) B2-B, (c) B2-B, (d) B3, (e) B6-A i (f) B6-B

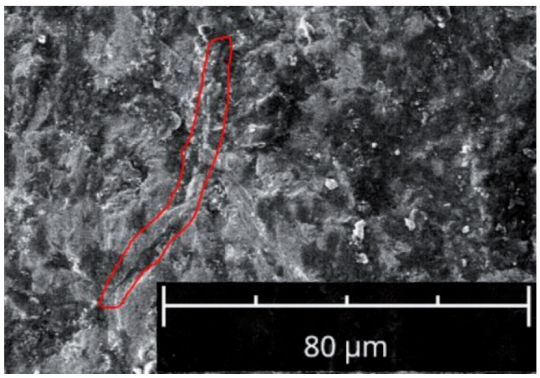

Fig. 12. Exemplary image of a crack propagating along the dendrite boundaries
Rys. 12. Przykładowy obraz pęknięcia propagującego się wzdłuż granic dendrytów

intensive wear is aligned along the dendrites. The harder phases (primary carbides) tend to aggregate in the inter-dendritic regions; hence the wear is observably lower.

Hardness evaluation

The hardness measurement is shown in **Figure 16**. The hardness appeared to vary between 59 and 61 HRC with a tendency to decrease away from the surface, which is another confirmation of applied heat treatment. It can also be stated that due to the nature of the hardness curve, the wear may be more intensive with the passage of time.

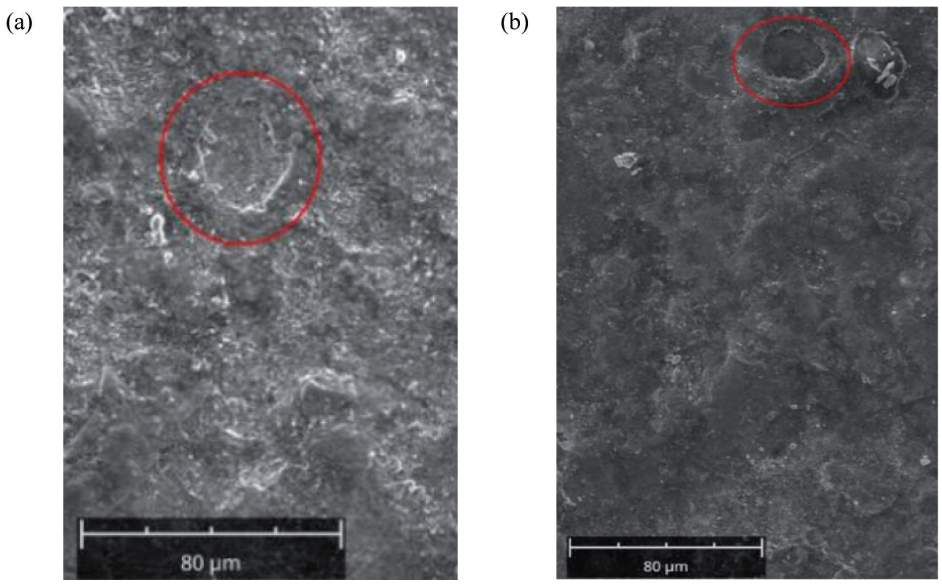

Fig. 13. Exemplary images of craters being a result of build-up ripping: (a) sample B4, (b) sample B5-B
Rys. 13. Przykładowe obrazy kraterów, będących wynikiem rozerwania narostu: (a) próbka B4, (b) próbka B5-B

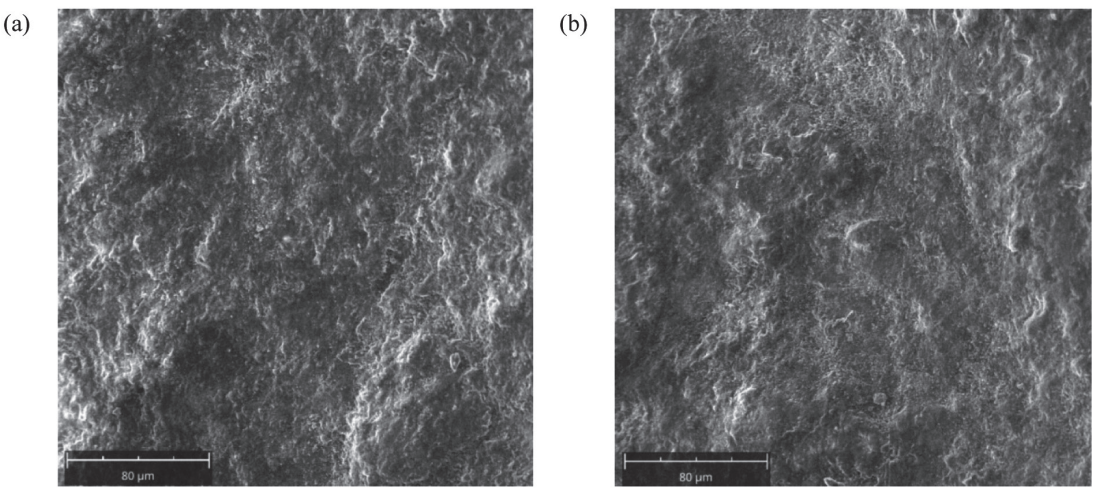

Fig. 14. Exemplary images of worn surface topography
Rys. 14. Przykładowe obrazy zużytej topografii powierzchni

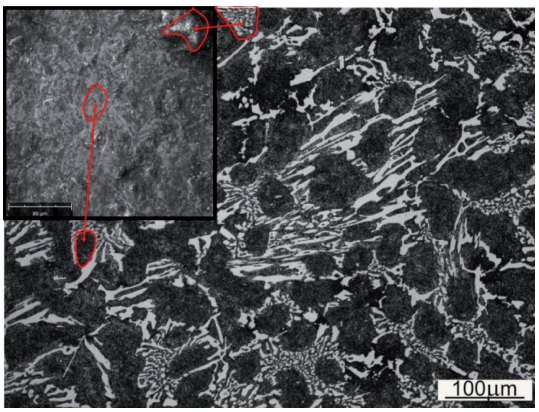

Fig. 15. Comparison of the same regions captured with SEM and metallographic microscope. The red areas with arrows represent the analogic regions of the studied sample

Rys. 15. Porównanie tych samych regionów uchwyconych za pomocą mikroskopu SEM i metalograficznego. Czerwone obszary ze strzałkami reprezentują analogiczne regiony badanej próbki

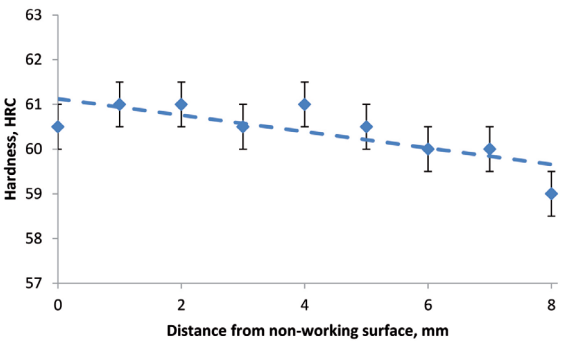

Fig. 16. Graph showing the decrease in hardness along the distance from non-working (thus not exploited) surface

Rys. 16. Wykres przedstawiający spadek twardości od nieeksploatowanej powierzchni

DISCUSSION

The wear resistance of the examined mantle lining can be differentiated into high and low particle kinetic energy resistance. The lattice of primary carbides is responsible for low particle kinetic energy, while the matrix withstands the deterioration caused by higher kinetic energies. In general, the material chosen for the lining fabrication is well fit to meet the operational requirements; however, the Authors found several casting-related issues, which caused casting defects. The defects may be responsible for limiting the possible lifespan of the gyratory crusher mantle lining. The first possible cause for the mantle wear is connected with the dualistic function of the carbides, whereas the first – advantageous – function is to provide high hardness and the second drawback is that the role is making the material prone to crack propagation along the grain boundaries. Unexpectedly, this effect comes primarily not from the exploitation but from casting mishandling, namely the uneven shrinkage. With that high carbon element content, the shrinkage generates cavities and micro-porosity, which enables crack propagation on the superficial layer of the lining. The cavities also decrease fatigue resistance since the half-torn husks of the surface have more degrees of freedom.

The uncommon, inclined wear ploughs are a possible result of the eccentric and rotational motion of the mantle.

Due to the high amount of chromium in the material of the mantle lining, the cost is noticeably higher than in the conventionally used Hadfield cast steel case. However, on the other hand, the high-manganese steel surface is prone to be damaged by the small particles with low impact energy **[L. 9]**, which can lead to uncontrolled and rapid erosion of the cone geometry. Contrastingly, the studied material does not exhibit such a strong dependency of its wear mechanism on the crushed particles' kinetics and size.

CONCLUSIONS

The multi-approach analyses above allow the Authors to draw several conclusions. Firstly, the chemical composition confirms the material as high-chromium cast iron, namely EN-GJN—HV600. The combined study of the microstructure, phase composition and hardness shows that the part has been subjected to heat treatment. The main components of the microstructure are M_7C_3 carbides and low-tempered martensite. The high amount of the primary carbides in the microstructure is formed as a continuous lattice.

There is a correlation between the local microstructure and local wear mechanisms – in the area where the carbide density is lower, as the part's surface is subjected to abrasive wear, whereas in areas of high carbide concentration, the dominant wear relies on crack propagation and resulting brittle fractures. The cracks tend to propagate away from the superficial layer along the crystallite boundaries, dendrites and the carbide lattice.

Acknowledgements

The authors thank Mr Dariusz Ryndak for his help during the research.

REFERENCES

1. Henckens T.: Scarce Mineral Resources: Extraction, Consumption and Limits of Sustainability. Resources, Conservation and Recycling 2021, 169, 105511, doi:10.1016/j.resconrec.2021.105511.
2. Rajan B., Singh D.: Investigation on Effects of Different Crushing Stages on Morphology of Coarse and Fine Aggregates. International Journal of Pavement Engineering 2020, 21, 177–195, doi:10.1080/10298436.2018.1449951.
3. Fladvad M., Onnela T.: Influence of Jaw Crusher Parameters on the Quality of Primary Crushed Aggregates. Minerals Engineering 2020, 151, 106338, doi:10.1016/j.mineng.2020.106338.
4. Johansson M., Bengtsson M., Evertsson M., Hulthén E.: A Fundamental Model of an Industrial-Scale Jaw Crusher. Minerals Engineering 2017, 105, 69–78, doi:10.1016/j.mineng.2017.01.012.
5. Revnivtsev V.I., Kapralov Ye.P., Finkelstein G.A., Zarogatsky L.P., Ivanov N.A., Blekhman I.I., Ivanov B.G.: Selective Liberation of Minerals in Inertial Cone Crushers. Powder Technology 1984, 38, 195–203, doi:10.1016/0032-5910(84)80050-9.
6. Evertsson M.: Cone Crusher Performance. 2015, doi:10.13140/RG.2.1.2212.7526.
7. Bengtsson M., Hulthén E., Evertsson C.M.: Size and Shape Simulation in a Tertiary Crushing Stage, a Multi Objective Perspective. Minerals Engineering 2015, 77, 72–77, doi:10.1016/j.mineng.2015.02.015.
8. Cepuritis R., Garboczi E.J., Jacobsen S.: Three Dimensional Shape Analysis of Concrete Aggregate Fines Produced by VSI Crushing. Powder Technology 2017, 308, 410–421, doi:10.1016/j.powtec.2016.12.020.
9 Bembenek M., Krawczyk J., Pańcikiewicz K.: The wear mechanism of mill beaters for coal grinding made-up from high manganese cast steel. Engineering Failure Analysis 2022, 142, 106843, https://doi.org/10.1016/j.engfailanal.2022.106843.
10. Gang D., Xiumin F., Dongming H.: Analysis and Optimization of Cone Crusher Performance. Minerals Engineering 2009, 22, 1091–1093, doi:10.1016/j.mineng.2009.03.020.
11. Lindroos M., Apostol M., Heino V., Valtonen K., Laukkanen A., Holmberg K., Kuokkala V.-T.: The Deformation, Strain Hardening, and Wear Behavior of Chromium-Alloyed Hadfield Steel in Abrasive and Impact Conditions. Tribol Lett 2015, 57, 24, doi:10.1007/s11249-015-0477-6.
12. Allende-Seco R., Artigas A., Bruna H., Carvajal L., Monsalve A., Sklate-Boja M.F.: Hardening by Transformation and Cold Working in a Hadfield Steel Cone Crusher Liner. Metals 2021, 11, 961, doi:10.3390/met11060961.
13. Petrov Y.N., Gavriljuk V.G., Berns H., Schmalt F.: Surface Structure of Stainless and Hadfield Steel after Impact Wear. Wear 2006, 260, 687–691, doi:10.1016/j.wear.2005.04.009.
14. Krawczyk J., Bembenek M., Pawlik J.: The Role of Chemical Composition of High-Manganese Cast Steels on Wear of Excavating Chain in Railway Shoulder Bed Ballast Cleaning Machine. Materials 2021, 14, 7794, doi:10.3390/ma14247794.
15. Johansson M., Quist J., Evertsson M., Hulthén E.: Cone Crusher Performance Evaluation Using DEM Simulations and Laboratory Experiments for Model Validation. Minerals Engineering 2017, 103–104, 93–101, doi:10.1016/j.mineng.2016.09.015.
16. Cleary P.W., Morrison R.D.: Geometric Analysis of Cone Crusher Liner Shape: Geometric Measures, Methods for Their Calculation and Linkage to Crusher Behaviour. Minerals Engineering 2021, 160, 106701, doi:10.1016/j.mineng.2020.106701.
17. Ma Y., Fan X., He Q.: Prediction of Cone Crusher Performance Considering Liner Wear. Applied Sciences 2016, 6, 404, doi:10.3390/app6120404.
18. Lindqvist M., Evertsson C.M.: Prediction of Worn Geometry in Cone Crushers. Minerals Engineering 2003, 16, 1355–1361, doi:10.1016/j.mineng.2003.08.011.
19. Lindqvist M., Evertsson C.M.: Development of Wear Model for Cone Crushers. Wear 2006, 261, 435–442, doi:10.1016/j.wear.2005.12.010.
20. Atabaki M.M., Jafari S., Abdollah-pour H.: Abrasive Wear Behavior of High Chromium Cast Iron and Hadfield Steel–A Comparison. J. Iron Steel Res. Int. 2012, 19, 43–50, doi:10.1016/S1006-706X(12)60086-7.

21. Klueh R.L., Maziasz P.J., Lee E.H.: Manganese as an Austenite Stabilizer in Fe Cr Mn C Steels. Materials Science and Engineering: A 1988, 102, 115–124, doi:10.1016/0025-5416(88)90539-3.
22. Ortega-Cubillos P., Nannetti-Bernardini P.A., Celso-Fredel M., Antonio Campos R.: Wear Resistance of High Chromium White Cast Iron for Coal Grinding Rolls. Rev. Fac. Ing. Antioquia 2015, doi:10.17533/udea.redin.n76a16.
23. Dumrudkarn C., Muangjunburee P.: Wear Behavior of Hardfacing Deposits on Hadfield Steel. KEM 2015, 658, 172–176, doi:10.4028/www.scientific.net/KEM.658.172.
24. Jilleh A., Kishore Babu N., Thota V., Anis A.L., Harun M.K., Talari M.K.: Microstructural and Wear Investigation of High Chromium White Cast Iron Hardfacing Alloys Deposited on Carbon Steel. Journal of Alloys and Compounds 2021, 857, 157472, doi:10.1016/j.jallcom.2020.157472.
25. Okechukwu C., Dahunsi O.A., Oke P.K., Oladele I.O., Dauda M.: Development of Hardfaced Crusher Jaws Using Ferro-Alloy Hardfacing Inserts and Low Carbon Steel Substrate. 2018, 20.
26. Okechukwu C., Dahunsi O.A., Oke P.K., Oladele I.O., Dauda M.: Review on Hardfacing as Method of Improving the Service Life of Critical Components Subjected to Wear in Service. Nig. J. Tech. 2018, 36, 1095, doi:10.4314/njt.v36i4.15.
27. Krawczyk J.: The role of the microstructure in tribological wear of iron alloys. AGH University of Science and Technology Press, Dissertations, Monographs 274, Krakow 2013 (in Polish).